




## Single- and double-electron capture in intermediate-energy $H^+ + Mg$ collisions

J. W. Gao <sup>1</sup>, Y. Y. Qi,<sup>2</sup> Z. H. Yang <sup>1</sup>, Z. M. Hu,<sup>1,\*</sup> Y. W. Zhang <sup>3</sup>, Y. Wu,<sup>4,3</sup> J. G. Wang,<sup>4</sup> A. Dubois,<sup>5</sup> and N. Sisourat<sup>5</sup>

<sup>1</sup>Key Laboratory of Radiation Physics and Technology of Ministry of Education,  
Institute of Nuclear Science and Technology, Sichuan University, Chengdu 610064, China

<sup>2</sup>College of Data Science, Jiaying University, Jiaying 314001, China

<sup>3</sup>Center for Applied Physics and Technology, HEDPS, and School of Physics, Peking University, Beijing 100871, China

<sup>4</sup>Key Laboratory of Computational Physics, Institute of Applied Physics and Computational Mathematics, Beijing 100088, China

<sup>5</sup>Sorbonne Université, CNRS, UMR 7614, Laboratoire de Chimie Physique-Matière et Rayonnement, 75005 Paris, France



(Received 15 June 2021; revised 29 August 2021; accepted 13 September 2021; published 28 September 2021)

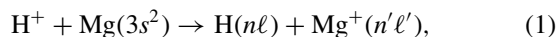
Single- and double-electron-capture processes occurring in the system of hydrogen ions colliding with alkaline-earth atoms,  $H^+ + Mg$ , are investigated in a broad energy domain ranging from 0.25 to 180 keV. Total and state-selective cross sections are calculated using a two-active-electron semiclassical asymptotic-state close-coupling approach. Our results show the best overall agreement with experimental data, and possible reasons for observed discrepancies are discussed. Comparison of our cross sections with previous theoretical results further demonstrates the importance of electronic correlations between the magnesium valence electrons and the strong couplings between various important channels. Furthermore, our investigations suggest that the oscillatory structures observed in the double-electron-capture cross sections stem from complex coherence effects between double-electron capture, electron transfer to excited states, and transfer-excitation processes.

DOI: [10.1103/PhysRevA.104.032826](https://doi.org/10.1103/PhysRevA.104.032826)

### I. INTRODUCTION

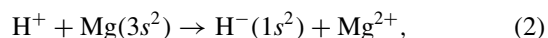
The study of hydrogen ions colliding with alkaline-earth atoms and detailed knowledge of the cross sections for various electronic processes occurring in such systems present interest for various domains such as astrophysics, fusion plasma, and nuclear physics [1–5]. From a fundamental point of view, such collision systems are also of challenging importance in relation to the effects of the electronic correlation between the two valence electrons of the target in the collision process.

A prototypical example from this class of problem is the  $H^+ + Mg$  collision system. For single-electron-capture (SEC) processes,



total cross sections were previously measured by Il' in *et al.* [6] in the energy range of 10–180 keV, by Futch and Moses [7] from 4 to 50 keV, by Berkner *et al.* [8] from 5 to 70 keV, by Morgan and Eriksen [9] from 1 to 100 keV, by Cisneros *et al.* [10] from 1 to 5 keV, by DuBois and Toburen [11] from 2 to 100 keV, and by Shah *et al.* [12] from 90 to 500 keV. Although this collision system has been extensively studied, only a single series of experimental data exists for state-selective SEC processes, i.e., SEC to  $H(2s)$  [13].

For the double-electron-capture (DEC) process,



investigations are more scarce. Furthermore, the existing experimental data [7,9,14] show that the DEC cross sections

oscillate at low impact energies, for which a complete explanation is still missing.

On the theoretical side, besides simple models proposed in the 1970s (see [9] and references therein), both total SEC and DEC cross sections for  $E < 10$  keV were calculated using a three-state molecular-orbital close-coupling (MOCC) method [15] and a multichannel Landau-Zener model [16] for which large discrepancies exist with the experimental data. The authors of [15] also performed classical-trajectory Monte Carlo (CTMC) calculations extending total SEC cross sections to higher energies, up to 40 keV. Later, extended MOCC calculations including 14 molecular states were performed for SEC processes for impact energies from 0.1 to 10 keV by Dutta *et al.* [17]: the results agree fairly well with experimental data above 3 keV, while at lower energies their cross sections are larger than the measurements. More recently, both total and state-selective SEC cross sections were calculated using the semiclassical impact-parameter close-coupling method [18] and CTMC method [19] in the energy ranges of 1–500 and 1–100 keV, respectively. However, these two independent investigations are in poor agreement with available measurements for impact energies below 3 keV. To date, detailed modeling and understanding of SEC processes in  $H^+ + Mg$  collisions are still required, and much less is known about the DEC process.

In this work, we theoretically study single- and double-electron-capture processes occurring in  $H^+ + Mg$  collisions for a wide energy domain ranging from 0.25 to 180 keV. We use a two-active-electron semiclassical asymptotic-state close-coupling (SCASCC) method with large basis sets, ensuring controlled convergence of the cross sections and providing physical insight into this collision system. Both

\*huzhimin@scu.edu.cn

total and state-selective SEC as well as DEC cross sections are presented and compared with available theoretical and experimental results. Possible reasons for the disagreements with existing data are also discussed. Furthermore, our investigation suggests an explanation for the oscillatory structures observed in the DEC cross sections.

The present paper is organized as follows. In the next section we briefly outline the SCASCC method used in the present calculations. Section III is devoted to a detailed analysis of the total and state-selective SEC as well as DEC cross sections, including direct comparisons with available experimental and theoretical results. They are followed by the conclusions in Sec. IV. Atomic units are used throughout, unless explicitly indicated otherwise.

## II. THEORY

In the present work, the cross sections of the electronic processes occurring during  $H^+ + Mg$  collisions are calculated by a two-active-electron SCASCC approach which was previously described, for example, in [22–24]. We outline only briefly the main features of the method. The two-electron time-dependent Schrödinger equation is written as

$$\left[ H_e - i \frac{\partial}{\partial t} \right] \Psi(\vec{r}_1, \vec{r}_2, t) = 0, \quad (3)$$

where  $H_e$  is the electronic Hamiltonian,

$$H_e = \sum_{i=1,2} \left[ -\frac{1}{2} \nabla_i^2 + V_T(r_i) + V_P(r_i^P) \right] + \frac{1}{|\vec{r}_1 - \vec{r}_2|}, \quad (4)$$

and  $\vec{r}_i$  and  $\vec{r}_i^P = \vec{r}_i - \vec{R}(t)$  are the position vectors of the electrons with respect to the target and the projectile, respectively. The relative projectile-target position  $\vec{R}(t)$  defines the trajectory, with  $\vec{R}(t) = \vec{b} + \vec{v}t$  being in the usual straight-line, constant-velocity approximation, where  $\vec{b}$  and  $\vec{v}$  are the impact parameter and velocity, respectively (see Fig. 1). The potentials  $V_T$  and  $V_P$  describe, respectively, the interaction between the electrons and the target and projectile nucleus, including inner electrons if the frozen-core approximation is used (see later).

The Schrödinger equation is solved by expanding the wave function onto a basis set composed of states of the isolated collision partners,

$$\begin{aligned} \Psi(\vec{r}_1, \vec{r}_2, t) = & \sum_{i=1}^{N_{TT}} c_i^{TT}(t) \Phi_i^{TT}(\vec{r}_1, \vec{r}_2) e^{-iE_i^{TT}t} \\ & + \sum_{j=1}^{N_{PP}} c_j^{PP}(t) \Phi_j^{PP}(\vec{r}_1, \vec{r}_2, t) e^{-iE_j^{PP}t} \\ & + \sum_{k=1}^{N_T} \sum_{l=1}^{N_P} c_{kl}^{TP}(t) [\phi_k^T(\vec{r}_1) \phi_l^P(\vec{r}_2, t) \\ & \pm \phi_k^T(\vec{r}_2) \phi_l^P(\vec{r}_1, t)] e^{-i(E_k^T + E_l^P)t}, \end{aligned} \quad (5)$$

where the superscripts  $T$  and  $TT$  ( $P$  and  $PP$ ) denote states and corresponding energies for which one and two electrons are on the target (projectile), respectively. The  $+$  and  $-$  in

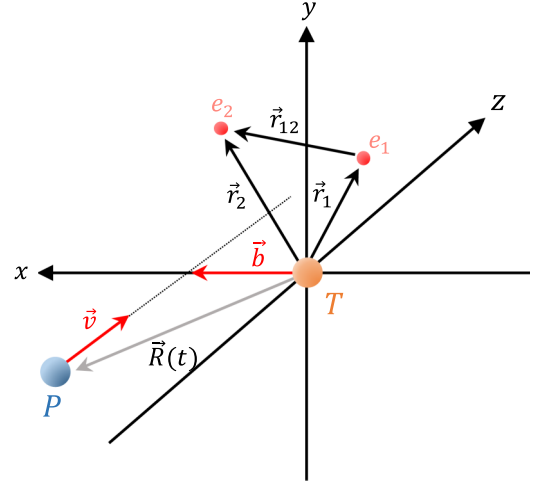


FIG. 1. Collision geometry. The impact parameter  $\vec{b}$  and velocity  $\vec{v}$  define the collision plane ( $xz$ ), and  $\vec{R}(t)$  defines the projectile (P) trajectory with respect to the target (T). The positions of two electrons with respect to the target center are denoted  $\vec{r}_1$  and  $\vec{r}_2$ , and  $\vec{r}_{12}$  is the relative vector between the two electrons. Note that for clarity we locate the origin of the reference on the target; this does not restrict the generality of our results, which are Galilean invariant.

the last part of Eq. (5) stand for the singlet and triplet spin states, respectively, and the wave functions  $\Phi_i^{TT}$  and  $\Phi_j^{PP}$  are related to the corresponding symmetry. For both electrons, the projectile states contain plane-wave electron translation factors  $e^{i\vec{v}\cdot\vec{r}_i - i\frac{1}{2}v^2t}$ , ensuring Galilean invariance of the results. The insertion of Eq. (5) into (3) results in a system of first-order coupled differential equations, which can be written in matrix form as

$$i \frac{d}{dt} \mathbf{c}(t) = \mathbf{S}^{-1}(\vec{b}, \vec{v}, t) \mathbf{M}(\vec{b}, \vec{v}, t) \mathbf{c}(t), \quad (6)$$

where  $\mathbf{c}(t)$  is the column vector of the time-dependent expansion coefficients, i.e.,  $c^{TT}$ ,  $c^{PP}$ , and  $c^{TP}$  in Eq. (5), and  $\mathbf{S}$  and  $\mathbf{M}$  are the overlap and coupling matrices, respectively. These equations are solved using the predictor-corrector, variable-time-step Adams-Bashford-Moulton method for a set of initial conditions: initial state  $i$  and given values of  $b$  and  $v$ . The probability of a transition  $i \rightarrow f$  is given by the coefficients  $c_f$  ( $\equiv c^{TT}$ ,  $c^{PP}$ , or  $c^{TP}$ ) as

$$P_{fi}(b, v) = \lim_{t \rightarrow \infty} |c_f(t)|^2. \quad (7)$$

The corresponding integral (total) cross sections for the considered transition are calculated as

$$\sigma_{fi}(v) = 2\pi \int_0^{+\infty} b P_{fi}(b, v) db. \quad (8)$$

In this work, for  $H^+ + Mg$  collisions, the method presented above is used for the electronic Hamiltonian  $H_e$  defined in Eq. (4) with

$$V_T(r_i) = -\frac{1}{r_i}, \quad V_P(r_i^P) = -\frac{2}{r_i^P} - \frac{10}{r_i^P} (1 + \alpha r_i^P) e^{-\beta r_i^P}, \quad (9)$$

where  $V_T$  corresponds to  $H^+$  and  $V_P$  corresponds to the  $Mg^{2+}$  ion in the frozen-core electron approximation in which the

TABLE I. Energies (in a.u.) of one- and two-electron states of the target ( $\text{Mg}^+$  and  $\text{Mg}$ ) and the projectile ( $\text{H}$  and  $\text{H}^-$ ) obtained in this work, compared with energies from NIST [20] and Ref. [21]. The values of energies for the target (projectile) are given relative to the  $\text{Mg}^+$  ( $\text{H}$ ) first ionization threshold, where the ionization potential (IP) = 0.553 a.u. (IP = 0.500 a.u.).

$\text{Mg}^+$			$\text{Mg}$			$\text{H}$			$\text{H}^-$		
State	This study	[20]	State	This study	[20]	State	This study	[20]	State	This study	[21]
$3s$	-0.552	-0.553	$^1S\ 3s^2$	-0.833	-0.834	$1s$	-0.500	-0.500	$^1S\ 1s^2$	-0.526	-0.528
$3p$	-0.389	-0.390	$^1P\ 3s3p$	-0.671	-0.674	$2s$	-0.125	-0.125			
$3d$	-0.224	-0.227	$^1D\ 3s3d$	-0.615	-0.622	$2p$	-0.125	-0.125			
$4s$	-0.235	-0.234	$^1S\ 3s4s$	-0.635	-0.635	$3s$	-0.055	-0.056			
$4p$	-0.184	-0.185	$^1P\ 3s4p$	-0.607	-0.608	$3p$	-0.055	-0.056			
$5s$	-0.129	-0.130	$^1S\ 3s5s$	-0.568	-0.594	$4s$	-0.031	-0.031			
						$4p$	-0.031	-0.031			
						$5s$	-0.020	-0.020			
						$5p$	-0.020	-0.020			

inner-shell electrons are assumed to be inactive. The interaction of these frozen electrons and the nucleus with the two active ones is described by the model potential. For the latter, the variational parameters  $\alpha = 2.128$  and  $\beta = 4.256$  were obtained through an optimization procedure in order to reproduce the  $\text{Mg}^+$  spectrum and  $\text{Mg}$  singlet spectrum (see Table I).

In our calculations, the one- and two-electron states included in the expansion, Eq. (5), are expressed in terms of Gaussian-type orbitals (GTOs) and products of these GTOs. For the system under consideration, a set of 56 GTOs (12 for  $l = 0$ ,  $8 \times 3$  for  $l = 1$ , and  $4 \times 5$  for  $l = 2$ ) is used in the  $\text{Mg}$  center, and a set of 35 GTOs (11 for  $l = 0$  and  $8 \times 3$  for  $l = 1$ ) is used in  $\text{H}$ . This allows the inclusion of 1249 singlet states in total: 387 TT ( $\text{Mg}$ ), 623 TP ( $\text{Mg}^+$ ,  $\text{H}$ ), and 239 PP ( $\text{H}^-$ ) states. These states can describe elastic, excitation, single-electron-capture, and double-electron-capture channels, as well as ionization through the inclusion of pseudostates with energy lying above ionization thresholds. Ionization processes are not discussed in detail in the following. However, at these collision energies they can be coupled to electron-capture channels, and it is thus essential to account for ionization [25] in the calculations. The important one- and two-electron states of the target ( $\text{Mg}^+$  and  $\text{Mg}$ ) and the projectile ( $\text{H}$  and  $\text{H}^-$ ) are reported in Table I, in which good agreement with available data [20,21] can be seen.

The cross sections reported in the following have been compared with those obtained with a larger basis set built from 69 GTOs (14 for  $l = 0$ ,  $10 \times 3$  for  $l = 1$ , and  $5 \times 5$  for  $l = 2$ ) for the  $\text{Mg}$  target and 43 GTOs (13 for  $l = 0$  and  $10 \times 3$  for  $l = 1$ ) in the  $\text{H}$  center. This procedure, which involves a much larger computation time, was performed for only five typical energies, i.e., 0.25, 1, 9, 20.25, and 100 keV. The total SEC cross sections from these two sets agree with each other within 6% in the whole considered energy domain. For  $n\ell$ -selective SEC cross sections, the convergence for most cross sections was evaluated to be about 10% at intermediate energies and to be less than 20% in the lower- and higher-energy regions. Only the cross sections for the weakest channels, i.e., the  $\text{H}(1s) + \text{Mg}^+(3s)$  and  $\text{H}(1s) + \text{Mg}^+(5s)$  channels at the lowest impact energies (0.25 keV), differ from each other by up to a factor of 1.5. For the DEC process, the cross sections differ

by less than 26% at the lowest impact energies and by less than 15% at the intermediate and high impact energies.

### III. RESULTS AND DISCUSSION

#### A. Total single-electron-capture cross sections

Our total-electron-capture cross sections are presented as a function of impact energy in Fig. 2(a), together with experimental data [6–9,11,12] and data from previous theoretical works [15,17–19]. Note that the cross sections for energies ranging from 0.25 to 10 keV are also presented in Fig. 2(b) on a linear scale for simpler comparison. Our cross sections reach a maximum around 9 keV and fall off rapidly with increasing impact energy, while a plateau-like structure is shown for  $E < 3$  keV. The latter structure comes from the interplay of electron transfer to excited states and transfer excitation processes, as shown in the next section (Figs. 3 and 4). The comparison with the previous results shows that the experimental results do not agree with each other. For example, at 2 keV results from [9,11] show a 37% difference and do not agree within their respective error bars. Around the maximum, the data from [7,8] agree with each other but are about 30% lower than those of [9,11]. For the highest energies shown in Fig. 2 the results of [6,12] differ by one order of magnitude. This fact, as well as the differences observed between theoretical data for energies lower than 5 keV, demonstrates the importance of new results for that collision system. Our cross sections agree with some of the experimental ones in the entire energy range, except above 70 keV, where they are lower than those of [9,11,12]. The latter discrepancy is certainly due to the fact that we use the frozen-core approximation, leaving the target inner-shell electrons passive. To support our interpretation we have simulated the capture process from the  $2s$  subshell of  $\text{Mg}$ , using our two-active-electron SCASCC method with the same basis sets and the model potential [we mention that the energies for  $\text{Mg}^+(2s)$  and  $\text{Mg}(2s^2)$  are  $-3.455$  and  $-5.653$  a.u., respectively]. The cross sections for  $2s$  electron capture to  $\text{H}(n\ell) + \text{Mg}^+(2s)$  are presented in Fig. 2. Indeed, the contribution from the capture of inner-shell electrons becomes non-negligible for high impact energies: for the  $2s$  electrons our calculated cross sections show a maximum around 100 keV, where, indeed, a change in slope is shown in the

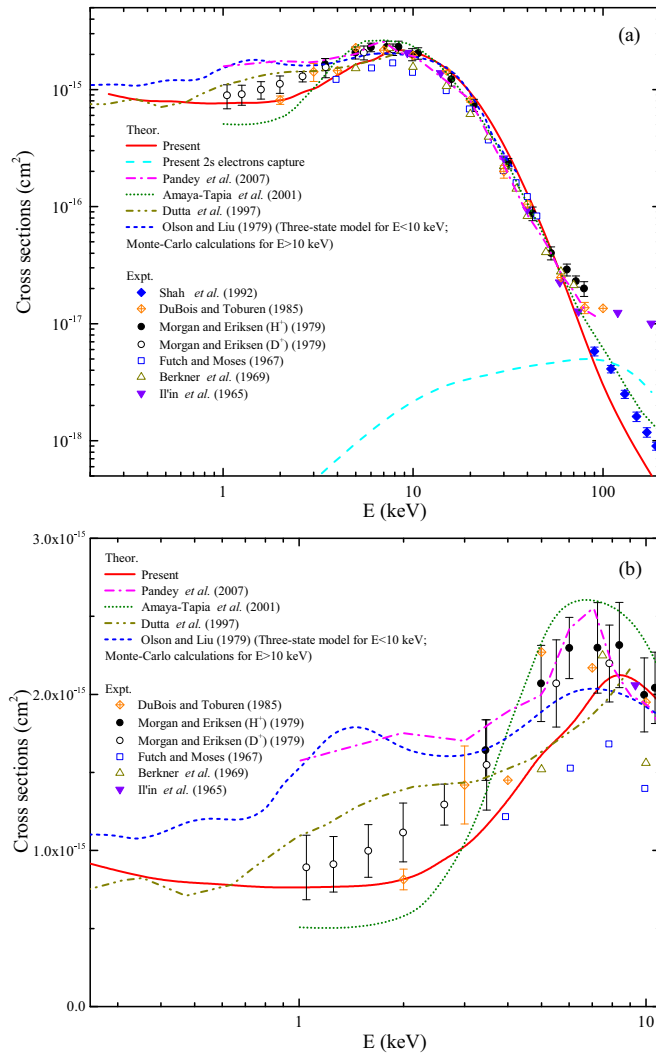


FIG. 2. (a) Total single-electron-capture cross sections as a function of the impact energy. The theoretical results are from the present calculations (red solid line), Pandey *et al.* [19] (pink dash-dotted line), Amaya-Tapia *et al.* [18] (green dotted line), Dutta *et al.* [17] (dark yellow dash-double-dotted line), and Olson and Liu [15] (blue short-dashed line). The present calculations for  $2s$  electron capture are also presented (cyan long-dashed line). The experimental results are from Shah *et al.* [12] (blue solid diamonds), DuBois and Toburen [11] (orange crossed diamonds), Morgan and Eriksen [9] (black solid circles), Futch and Moses [7] (blue open squares), Berkner *et al.* [8] (dark yellow open triangles) and Il'in *et al.* [6] (purple downward solid triangles). Note that experimental data from [9] for  $D^+$  ions (black open circles) are plotted at the  $\frac{1}{2} D^+$  energy. (b) Same as (a), but for energies ranging from 0.25 to 10 keV on a linear scale.

experimental results [6,9,11] and in a weaker way in [12]; for the  $2p$  target electrons, which are less bound than the  $2s$  ones, the maximum of the capture of these electrons is expected to be located at a lower energy, hidden in the predominant capture from the valence electrons.

We also compare our results with other theoretical works. Our total SEC cross sections are in good agreement with the results of Olson and Liu [15] and MOCC calculations of Dutta *et al.* [17] for energies above 5 keV. It is interesting to note that

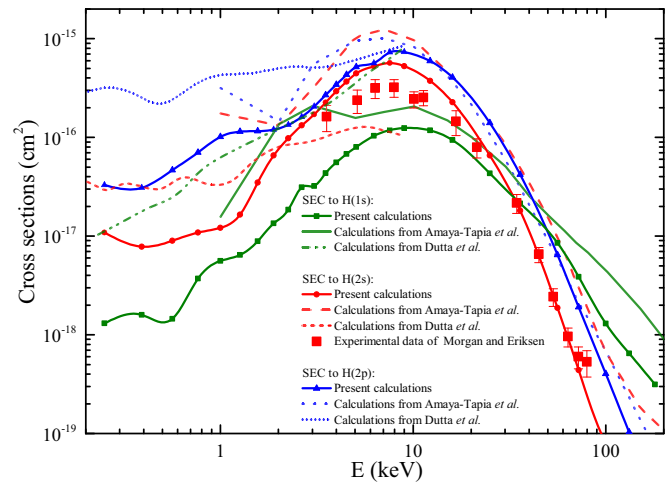


FIG. 3. Cross sections for SEC into  $H(1s)$  (green),  $H(2s)$  (red), and  $H(2p)$  (blue), while the target remains in the ground state  $Mg^+(3s)$ . The present calculations are plotted as solid lines with symbols; theoretical results from Dutta *et al.* [17] for SEC into  $H(1s)$ ,  $H(2s)$ , and  $H(2p)$  are denoted as dash-double-dotted, short-dashed, and dotted lines, respectively; theoretical results from Amaya-Tapia *et al.* [18] for SEC into  $H(1s)$ ,  $H(2s)$ , and  $H(2p)$  are presented as solid, long-dashed, and dotted lines, respectively. The experimental results of Morgan and Eriksen [13] (squares) for capture to  $H(2s)$  are also shown.

the results of Pandey *et al.* [19] and Amaya-Tapia *et al.* [18] lie below ours in this range but get larger beyond 70 keV, where they agree better with experimental data [9,11,12]. We believe that the differences from our results are due to different reasons: (i) the use of a single active electron with a model potential to describe the interaction between a  $Mg^+$  ion and a single electron (i.e., electron-electron correlation and electron exchange effects were not taken into account) and (ii) the use of an overestimation of the SEC by the use of an approximate binomial distribution [26]. One can see, indeed, that in [18]

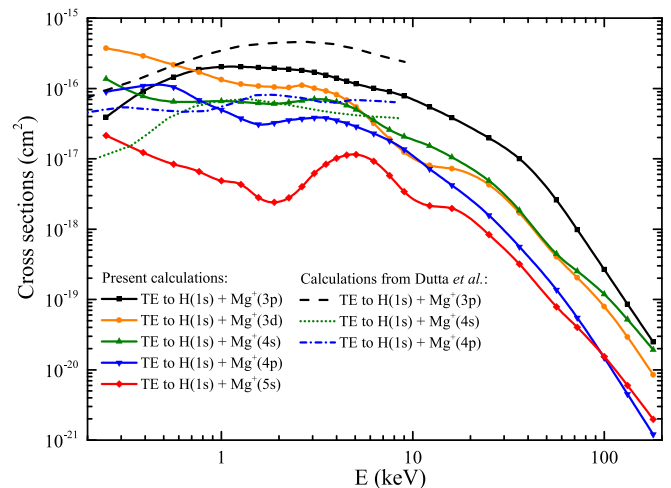


FIG. 4. Cross sections for TE processes. The present calculations are plotted as solid lines with symbols; theoretical results from Dutta *et al.* [17] for TE to  $Mg^+(3p)$ ,  $Mg^+(4s)$ , and  $Mg^+(4p)$  are denoted as long-dashed, dotted, and dash-dotted lines, respectively.

the cross sections for selective electron capture are overestimated compared to our results and the experimental data of Morgan and Eriksen [13] (see Fig. 3). The agreement of the results in [18] with the experimental data of Shah *et al.* [12] is therefore certainly due to a compensation effect between the overestimation of these cross sections and the failure to take into account the transfer of inner-shell electrons, processes which are not negligible in this energy domain (see above).

For low energies, say  $E < 3$  keV, the available theoretical results differ significantly. On the one hand, the CTMC calculations of Pandey *et al.* [19] overestimate experimental data [9,11], reaching a factor of 2 disagreement at 1 keV; it is known that the CTMC method, independent of the employed initial distribution, cannot reproduce accurate capture cross sections for low energies since it presents serious limitations to describing molecular features, as pseudocrossings [27]. Note that the three-state MOCC calculations of Olson and Liu [15] also overestimate our results and the experimental data [9,11]. On the other hand, the results from Amaya-Tapia *et al.* [18] underestimate the data [9,11]; this disagreement is most likely caused by the lack of representation of transfer excitation (TE) channels in their single-active-electron approach: TE plays an important role in the SEC processes at lower impact energies (see Fig. 4). The calculations of Dutta *et al.* [17], which include 14 molecular states, show good agreement with ours for energies lower than 0.7 keV and higher than 5 keV. However, for energies in between, their results exceed ours by up to 70%. As reported in [17], Dutta *et al.* examined the convergence of their results by increasing the molecular states involved in the calculations from 3 to 14, but the convergence is not monotonic (see Fig. 5 in [17]). Note again that we included 1249 channels in our calculations, for which the convergence has also been checked and is better than 6% for the present total SEC cross sections. We emphasize that, in this energy region ( $E < 3$  keV), our two-active-electron calculations, taking into account both electronic correlations between the two valence electrons and important one- and two-electron channels, show the best overall agreement with available experimental data [9,11].

### B. $n\ell$ -selective single-electron-capture cross sections

We now investigate state-selective SEC cross sections to provide detailed information on the final-state distribution of captured electrons, which is of particular interest both in astrophysics and in plasma diagnostics research since it determines the characteristics of the emitted radiation.

In Fig. 3 we provide the cross sections for SEC into ground state H(1s) and excited L-shell H(2s) and H(2p), while the target is in the ground state Mg<sup>+</sup>(3s). The experimental data from Morgan and Eriksen [13] and theoretical results of Amaya-Tapia *et al.* [18] and Dutta *et al.* [17] are also presented for comparison. From Fig. 3, it is clear that there is no agreement between the presented results. Indeed, our results show that electron transfer to H(2p) is dominant below 50 keV, while SEC to H(1s) takes over for higher energies. As can be observed in Fig. 3, the MOCC calculations of Dutta *et al.* [17] are in rather poor agreement with our results as well as the theoretical results of Amaya-Tapia *et al.* [18] and the experimental data [13] for electron transfer to H(2s). Moreover,

the calculations of Dutta *et al.* [17] overestimate significantly the dominant SEC to H(2p) process for lower impact energies. This explains the overestimation of the total SEC of the results obtained by these authors observed in Fig. 2. The calculations of Amaya-Tapia *et al.* always lie above our results, except for electron transfer to H(2p) for energies at 15–60 keV, for which their results lie slightly below ours. The most likely reason for the discrepancies is the use of the independent electron approximation.

Comparing our results with the only existing experimental data from [13] for electron transfer to H(2s), we obtain very good agreement for energies ranging from 20 to 70 keV but then underestimate the data for higher energies. The latter disagreement may be due again to the frozen-core approximation employed in our calculations. For energies from 3 to 20 keV, our results are larger than the experimental data, within a factor of 2. We cannot make a firm conclusion about this discrepancy, although the convergence of the present calculation has been checked, as mentioned above, to be about 10% at this energy range. In addition, as mentioned in [13], the absolute uncertainty of the experimental data was difficult to assess owing to possible systematic errors associated with the calibration of the Lyman- $\alpha$  detector and in the evaluation of the metal vapor pressure from thermodynamic data. Further experimental investigations will be useful to draw definite conclusions.

In Fig. 4, we present the cross sections for the TE process, which is actually a two-electron process, i.e., the transfer of one electron to the ground state of the projectile while the second target electron is excited. The MOCC calculations of Dutta *et al.* [17] are also presented. Compared to the processes with the transfer to excited states shown in Fig. 3, the TE cross sections show a very different behavior as a function of impact energy: all considered TE processes, except TE to Mg<sup>+</sup>(3p), decrease with increasing energy, showing oscillatory structures for energies below 30 keV. This tends to indicate that they are strongly coupled. Furthermore, the respective decrease and increase of the contributions of the transfer to excited states and TE for energies lower than 3 keV result in the plateaulike structure in the total SEC cross sections (see Fig. 2). A comparison of our calculated TE cross sections with the only available calculations of Dutta *et al.* [17] shows large discrepancies. To our knowledge, no experimental investigation is available to confirm one or the other series of predictions. However, it should be noted that the calculations in [17] considered only 14 molecular states, and their convergence is not monotonic, while we included 1249 channels in our calculations.

### C. Double-electron-capture cross sections

In Fig. 5, our DEC cross sections are presented and compared with available experimental data [7,9,14,28] as well as the unique available calculations based on a multichannel Landau-Zener model [16]. It can be seen that the measured DEC cross sections are more than one order of magnitude smaller than the SEC ones, showing, moreover, a clear oscillatory structure. Our results reproduce well the experimental data [7,9,14] in both magnitude and shape, while the multichannel Landau-Zener calculations [16] significantly

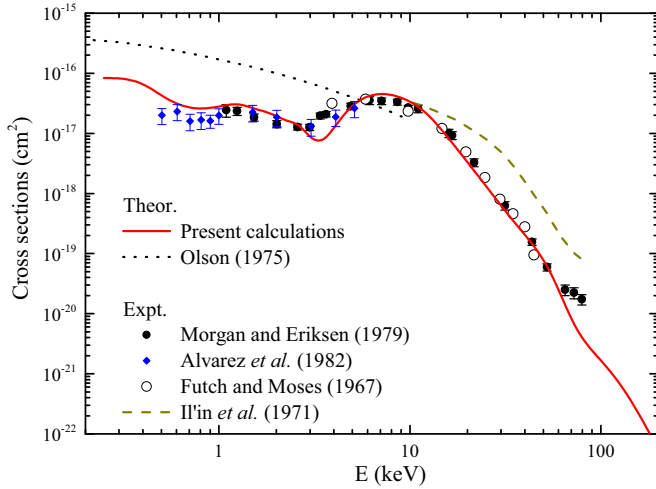


FIG. 5. Total DEC cross sections as a function of the impact energy. Theoretical results are from the present calculations (red solid line) and Olson [16] (black dotted line). The experimental results are from Morgan and Eriksen [9] (black solid circles), Alvarez *et al.* [14] (blue solid triangles), Futch and Moses [7] (black open circles), and Il'in *et al.* [28] (dark yellow dashed line).

exceed the measured data and do not reproduce the observed oscillatory structure. Note that above 70 keV, our results underestimate the measured data [9] as in the case of SEC (see Fig. 2). This is again certainly due to the frozen-core approximation employed in our calculations and to a non-negligible DEC process involving inner and valence electrons. It should also be noted that the experimental results of Il'in *et al.* [28] lie above our calculations and do not agree with the other available experimental data [7,9,14].

We have further investigated the oscillatory structure in the DEC cross sections based on our *ab initio* calculations. In the following, we show the cross sections for DEC and some specific channels which also present oscillations in the same energy range as DEC. In the same manner as in [29], to show the oscillatory structure more clearly, we present in Fig. 6(a) the cross sections of the DEC process as a function of the inverse of the relative velocity  $1/v$ , together with electron transfer to  $H(2p_{\pm 1}) + Mg^+(3s)$  and those corresponding to two-electron TE processes, i.e., transfer of one electron to the ground state of the projectile  $H(1s)$  while the second target electron is excited to  $Mg^+(3d_{\pm 1})$  and  $Mg^+(4p_0)$ . The cross sections for DEC and TE to  $H(1s) + Mg^+(3d_{\pm 1})$ , as well as electron transfer to  $H(2p_{\pm 1}) + Mg^+(3s)$  and TE to  $H(1s) + Mg^+(4p_0)$ , show clear periodic oscillations but with opposite phases. This suggests that the oscillatory patterns come from coherence effects between the considered DEC, TE, and electron transfer processes. In fact, such oscillatory structure in total cross sections was observed previously for symmetric collision systems and was interpreted by a three-state two-crossing model proposed by Rosenthal and Foley [30]: (i) for excitation of helium by helium-ion impact (see [31] for more details on the model), (ii) for ionization and negative-ion formation in  $H + H$  collisions [32], and (iii) recently, for double-electron capture in  $H^+ + H^-$  collisions [29]. In the present asymmetric collision system,

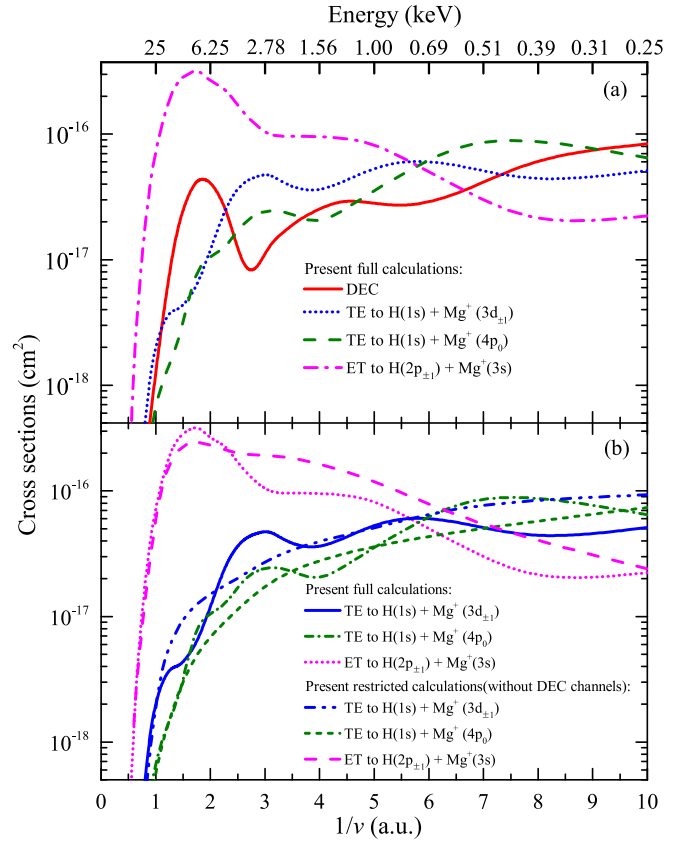


FIG. 6. (a) The present cross sections as a function of the inverse of the relative velocity  $1/v$  for DEC, electron transfer to  $H(2p_{\pm 1}) + Mg^+(3s)$ , and TE to  $Mg^+(3d_{\pm 1})$  and  $Mg^+(4p_0)$  channels. (b) Comparison of electron transfer and TE cross sections obtained from the present full two-active-electron calculations and restricted two-active-electron calculations without DEC channels (see text).

the interference mechanism, involving DEC, TE, and electron transfer to excited-state channels, is more complex than that from the Rosenthal model because of the rich molecular energy curves observed for this system [33]. To support our interpretation of the oscillatory structures, additional restricted two-active-electron calculations, i.e., with the same close-coupling scheme and basis set but excluding DEC channels, have been performed: cross sections for electron transfer to  $H(2p_{\pm 1}) + Mg^+(3s)$  and TE to  $Mg^+(3d_{\pm 1})$  and  $4p_0$  are presented and compared with the results from our full calculations in Fig. 6(b). One can observe that the calculations with and without DEC channels agree with each other in magnitude but not in shape: indeed, the cross sections from our restricted calculations (without DEC channels) show a quite smooth behavior without oscillatory energy-dependent structures. This reinforces the interpretation that the oscillatory structures observed in DEC cross sections stem from complex coherence effects between the processes for DEC, TE, and electron transfer to excited states. However, to our knowledge, state-to-state cross sections for TE processes and electron transfer to higher excited states of the projectile have never been reported experimentally, and theoretical calculations using the MOCC method including all important channels are also not available. Further experimental and theoretical investigations will be useful to draw definite conclusions.

#### IV. CONCLUSION

In this work, single- and double-electron-capture processes occurring in  $H^+ + Mg$  collisions have been investigated in a wide collision energy region from 0.25 to 180 keV. We used a two-active-electron SCASCC method with a large basis set to reach controlled reasonable convergence. To date, our close-coupling description of the collision is the most elaborate one in terms of accounting for electron correlation and open channels. For total SEC and DEC cross sections, our calculations show the best overall agreement with experimental results, except for energies higher than 70 keV, for which our results are lower than experimental data. We showed that these discrepancies are certainly due to the frozen-core approximation employed in our calculations and tend to reflect the substantial contribution from inner-shell electron capture. Comparison of our results with other theoretical calculations further demonstrated the importance of strong couplings between various channels and electronic correlation effects. Apart from the total cross sections, the state-to-state electron transfer and TE cross sections were also reported and compared with avail-

able experimental and theoretical results. Whereas fairly good agreement is found with the only existing experimental data for electron transfer to  $H(2s)$ , there are large discrepancies between our results and other available calculations. Possible reasons for the latter discrepancies were also discussed. Furthermore, our investigations suggest that the oscillatory structures observed in the DEC cross sections stem from the coherence effect between processes for DEC, TE, and electron transfer to excited states. Further experimental investigations and molecular-orbital-based calculations taking care of all important channels are required to draw definite conclusions and confirm our interpretation.

#### ACKNOWLEDGMENTS

This work is supported by the National Natural Science Foundation of China (Grants No. 11934004 and No. 12004350), the National Key Research and Development Program of China (Grant No. 2017YFA0402300), and the Fundamental Research Funds for the Central Universities in China (Grants No. YJ202143 and No. YJ202144).

- 
- [1] T. J. Morgan, R. E. Olson, A. S. Schlachter, and J. W. Gallagher, *J. Phys. Chem. Ref. Data* **14**, 971 (1985).
- [2] P. S. Barklem, A. K. Belyaev, A. Spielfiedel, M. Guitou, and N. Feautrier, *Astron. Astrophys.* **541**, A80 (2012).
- [3] S. Alexeeva, T. Ryabchikova, L. Mashonkina, and S. Hu, *Astrophys. J.* **866**, 153 (2018).
- [4] M. Bacal, *Chem. Phys.* **398**, 3 (2012).
- [5] H. Paetz gen Schieck, *Nuclear Physics with Polarized Particles* (Springer, Berlin, 2012).
- [6] R. N. Il'in, V. A. Oparin, E. S. Solov'ev, and N. V. Fedorenko, *JETP Lett.* **2**, 197 (1965).
- [7] A. H. Futch, Jr., and K. G. Moses, in *Abstracts of Papers of "the Fifth International Conference on the Physics of Electronic and Atomic Collisions"* (Nauka, Leningrad, 1967), p. 12. Note that the values given in this reference have been multiplied by 0.81 to take into account the new thermodynamic evaluation given in Ref. [34] as reported in Ref. [9].
- [8] K. H. Berkner, R. V. Pyle, and J. W. Stearns, *Phys. Rev.* **178**, 248 (1969).
- [9] T. J. Morgan and F. J. Eriksen, *Phys. Rev. A* **19**, 1448 (1979).
- [10] C. Cisneros, H. Martínez, B. Fuentes, I. Alvarez, J. de Urquijo, and I. Dominguez, *Nucl. Instrum. Methods Phys. Res., Sect. B* **117**, 1 (1996).
- [11] R. D. DuBois and L. H. Toburen, *Phys. Rev. A* **31**, 3603 (1985).
- [12] M. B. Shah, P. McCallion, Y. Itoh, and H. B. Gilbody, *J. Phys. B* **25**, 3693 (1992).
- [13] T. J. Morgan and F. Eriksen, *Phys. Rev. A* **19**, 2185 (1979).
- [14] I. Alvarez, C. Cisneros, and A. Russek, *Phys. Rev. A* **26**, 77 (1982).
- [15] R. E. Olson and B. Liu, *Phys. Rev. A* **20**, 1366 (1979).
- [16] R. E. Olson, *Phys. Lett. A* **55**, 83 (1975).
- [17] C. Dutta, P. Nordlander, and M. Kimura, *Chem. Phys. Lett.* **264**, 51 (1997).
- [18] A. Amaya-Tapia, R. Hernández-Lamoneda, and H. Martínez, *J. Phys. B* **34**, 769 (2001).
- [19] M. K. Pandey, R. K. Dubey, and D. N. Tripathi, *Eur. Phys. J. D* **41**, 275 (2007).
- [20] A. Kramida, Yu. Ralchenko, J. Reader, and NIST ASD Team, NIST Atomic Spectra Database, version 5.8, <https://physics.nist.gov/asd>.
- [21] C. L. Pekeris, *Phys. Rev.* **112**, 1649 (1958).
- [22] N. Sisourat, I. Pilskog, and A. Dubois, *Phys. Rev. A* **84**, 052722 (2011).
- [23] J. W. Gao, Y. Wu, N. Sisourat, J. G. Wang, and A. Dubois, *Phys. Rev. A* **96**, 052703 (2017).
- [24] Y. W. Zhang, J. W. Gao, Y. Wu, F. Y. Zhou, J. G. Wang, N. Sisourat, and A. Dubois, *Phys. Rev. A* **102**, 022814 (2020).
- [25] Note that our results show that the ionization cross sections are about one order of magnitude smaller than SEC ones in the low-energy region, equal to SEC ones at 20 keV, and two orders of magnitude larger at 180 keV.
- [26] Instead of the standard  $2 \times P(1 - P)$  ( $P$  is the probability of capture evaluated in the one-electron calculations), Amaya-Tapia *et al.* [18] used  $2P$ , and Pandey *et al.* [19] used  $2P - P \times P$ .
- [27] L. F. Errea, F. Guzmán, C. Illescas, L. Méndez, B. Pons, A. Riera, and J. Suárez, *Plasma Phys. Control. Fusion* **48**, 1585 (2006).
- [28] R. N. Il'in, V. A. Oparin, I. T. Serenkov, S. E. Solov'ev, and N. V. Fedorenko, in *Abstracts of Papers of "Proceedings of the VII International Conference on the Physics of Electronic and Atomic Collisions"* (North Holland, Amsterdam, 1971), p. 793. Note that the data were reported in Ref. [9].
- [29] J. W. Gao, Y. Wu, J. G. Wang, A. Dubois, and N. Sisourat, *Phys. Rev. Lett.* **122**, 093402 (2019).

- [30] H. Rosenthal and H. M. Foley, *Phys. Rev. Lett.* **23**, 1480 (1969).
- [31] H. Rosenthal, *Phys. Rev. A* **4**, 1030 (1971).
- [32] S. Y. Ovchinnikov, Y. Kamyshkov, T. Zaman, and D. R. Schultz, *J. Phys. B* **50**, 085204 (2017).
- [33] N. Khemiri, R. Dardouri, B. Oujia, and F. X. Gadéa, *J. Phys. Chem. A* **117**, 8915 (2013).
- [34] R. Hultgren, P. D. Desai, and D. T. Hawkins, *Selected Values of the Thermodynamic Properties of the Elements* (American Society for Testing and Materials, Metals Park, OH, 1973).